Active Magnetoplasmonic Ruler

Irina Zubritskaya,*,[†] Kristof Lodewijks,[†] Nicolò Maccaferri,*,[‡] Addis Mekonnen,[†] Randy K. Dumas,[§] Johan Åkerman,[§,⊥] Paolo Vavassori,[‡,∥] and Alexandre Dmitriev*,[†]

[†]Department of Applied Physics, Chalmers University of Technology, Göteborg 41296, Sweden

[‡]CIC nanoGUNE, Donostia−San Sebastian 20018, Spain

[§]Department of Physics, University of Gothenburg, Gothenburg 412 96, Sweden

[∥]IKERBASQUE, Basque Foundation for Science, Bilbao 48011, Spain

[⊥]Materials Physics, School of Information and Communication Technology, KTH Royal Institute of Technology, 16440 Kista, Sweden

S Supporting Information

ABSTRACT: Plasmon rulers are an emerging concept in which the strong near-field coupling of plasmon nanoantenna elements is employed to obtain structural information at the nanoscale. Here, we combine nanoplasmonics and nano-magnetism to conceptualize a magnetoplasmonic dimer nanoantenna that would be able to report nanoscale distances while optimizing its own spatial orientation. The latter constitutes an active operation in which a dynamically optimized optical response per measured unit length allows for the measurement of small and large nanoscale distances with about 2 orders of magnitude higher precision than current state-of-the-art plasmon rulers. We further propose a concept to optically measure the nanoscale response to the controlled application of force with a magnetic field.

KEYWORDS: magnetoplasmonics, plasmon ruler, nickel, cobalt, localized surface plasmon resonance, magneto-optical Kerr effect (MOKE), dimer
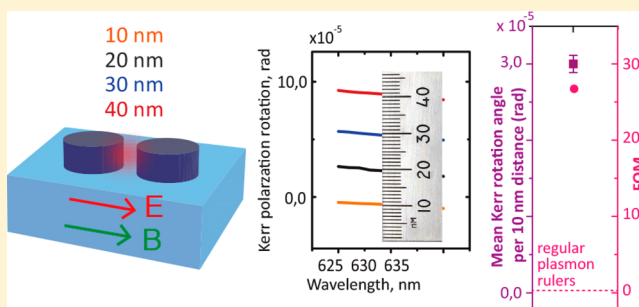
Accurate measurements of distances on the nanoscale are decisive in many aspects of the materials and life sciences. Prominent examples include studies of various biochemical processes via conformational changes in biomolecules. Previously, the optical tools used to obtain spatial information on the nanoscale, and down to the single-molecule level, focused on Förster resonance energy transfer (FRET) spectroscopy and the use of organic fluorophoresin so-called molecular rulers. Dynamic processes, such as DNA bending and cleavage and RNA catalysis and folding as well as protein−protein interactions, were all first explored by FRET. However, the limitation of fluorophores due to their photo bleaching and degradation over time led to the emergence of noble-metal nanoparticle-based plasmon rulers.[1−4] The operation of plasmon rulers relies on localized collective electronic oscillations (localized plasmons) in nanometal assemblies and on the near-field coupling (i.e., hybridization) between the plasmon modes of the adjacent nanoparticles, which strongly depends on the interparticle distance.[5,6] Plasmon local electromagnetic near-fields exponentially decay over distance, and as such, at small separations, the near-field enhancement and coupling effects increase dramatically. The underlying idea of a plasmon ruler, which consists of two or more noble metals or elements of core−shell structures, is then the extreme sensitivity of the light scattering to the interparticle gap

size.[5−12] This was first explored with nanoplasmonic dimer antennas almost a decade ago for monitoring the kinetics of single DNA hybridization events in solution.[1] In later realizations, plasmon rulers with subnanometer resolution consisted of thin-film coupled single-particle nanoantennas that utilized thiol monolayers with an adjustable chain length.[2] The principles of plasmon ruler design are typically refined with lithographically fabricated nanoantennas that are implemented to investigate the distance dependence of plasmon-coupling effects and to derive a plasmon ruler equation.[3] This includes the concept of a multielement three-dimensional plasmon ruler[4] to track the complex conformational changes that have also been recently realized in solution.[13]

Plasmonic antennas with magnetic functionality—for example, core−shell nanoparticles, typically with a magnetic oxide core—are often employed in theranostics[14] (i.e., therapy and diagnostics combined) and for magnetic targeting, on account of their ability to remotely guide the delivery of such functional nanoantennas via an externally applied magnetic field. However, such dual functionality has not actively been explored
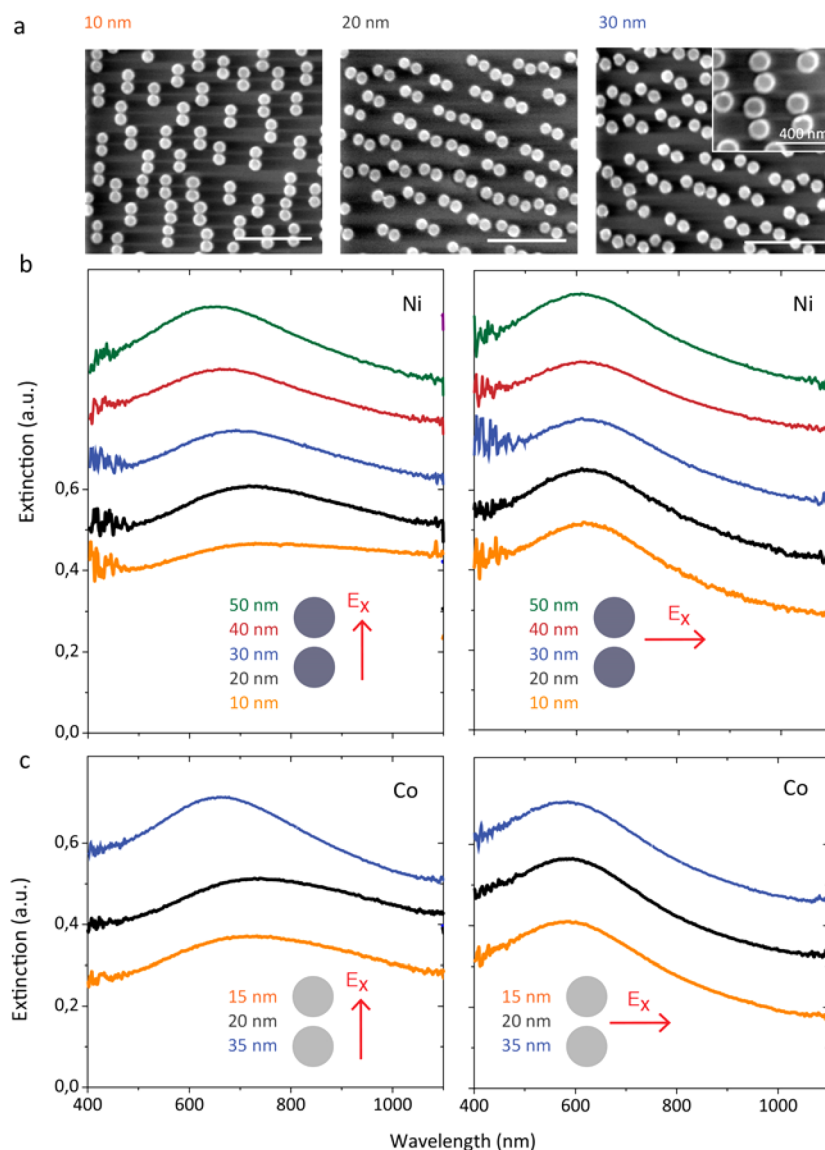
Figure 1. (a) Scanning electron microscopy (SEM) images of Ni magnetoplasmonic rulers with gap sizes of 10 nm (left), 20 nm (center), and 30 nm (right). Scale bars: 1 μm. (b) Extinction spectra of Ni rulers and (c) extinction spectra of Co rulers for orientations of the electric field along (left) and perpendicular to (right) the longitudinal ruler axis. Data shifted vertically for clarity of presentation.

to date with plasmon rulers. One very recent implementation used a magnetic core as a purification handle during the dimer plasmon ruler assembly, which in surface-bound plasmon dimer rulers results in improved theranostic sensitivity.[15]

In this work, we conceptualize the plasmon ruler with an active operation mode that we call *signal amplification by spatial orientation*. Such a ruler is built entirely of metallic ferromagnetic constituents, which also supports localized plasmon resonances: magnetoplasmonic nanoantennas (Figure 1a).[16] Thereabout nanoscale distances in such a ruler is performed via spectrally resolved magneto-optical Kerr effect (MOKE) rather than optical spectroscopy. As the former uses an externally applied magnetic field, the nanoscale distances are recorded on an entire ensemble of nominally identically oriented rulers, if they are free to reorient themselves in the medium and align the ruler axis parallel to the field. As we demonstrate below, the best rulers in terms of nanoscale resolution—that is, in terms of sensitivity and figure-of-merit— are indeed those addressed by both electric and magnetic fields,

oriented along the longitudinal (magnetically easy) axis of the dimer ruler.

We first probe the magnetoplasmonic ruler with conventional optical (extinction) spectroscopy. We take two archetypical magnetoplasmonic materials: Ni[17−21] and Co,[22,23] and fabricate large-scale short-range-ordered bottom-up arrays of nominally identically oriented nanodisk dimers with hole−mask colloidal lithography (HCL) (see Figure 1a for Ni ruler structure with various gaps and nanodisks in the dimers with nominal diameters of 150 nm and heights of 30 nm).[24] Interestingly, the HCL nanofabrication delivers a dimer ruler system that conceptually approaches the real solution-based ensemble for the measurement of nanoscale distances: due to bottom-up nanofabrication, the distances between individual rulers (and thus potential unwanted electromagnetic coupling between them) is averaged in the array (see Figure 1a). In the situation with spectroscopic averaging of the nanogap reading from a large number of rulers, this helps us to grasp the potential challenges that the usage of the ruler would

encounter in a real biochemical environment. The highly damped plasmon resonances in nanoscale ferromagnets, when hybridized, display rather broad spectral features both along the longitudinal (Figure 1b,c, left panels) and transversal (Figure 1b,c, right panels) axes of the ruler. The broad resonance shape prevents the strongly pronounced modification of the spectral optical response with varying gap size, as opposed to conventional plasmon rulers. For Ni rulers, we observe reasonably visible red shifts of the longitudinal hybrid plasmon resonance with decreasing gap size and a hint of a red shift of the tangential resonance with decreasing gap size (Figure 1b). In Co rulers, the same features in both resonances become even less evident due to the increased dielectric losses in the material (Figure 1c).

We further map the near-field and far-field optical responses of magnetoplasmonic rulers with a simple dipole−dipole model (see Supporting Information) and finite-difference time-domain (FDTD) simulations (Figure 2). Illuminating the dimer ruler
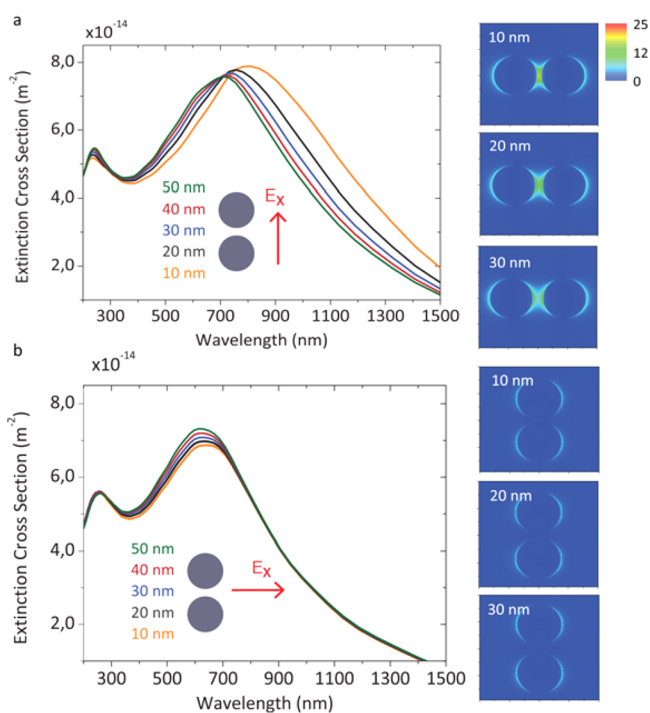
Figure 2. FDTD calculated far-field extinction spectra (left) and near-field response (right) for longitudinal (a) and transversal (b) plasmon modes of Ni magnetoplasmonic rulers with various nanogaps.

along the longitudinal axis promotes the emergence of the so-called bonding mode (lowest order hybridized mode in coupled dipole/bow-tie antennas) in the visible spectral range (see the schematics of induced charge for this hybrid mode in Figure S2a of the Supporting Information), generating a reasonably strong near-field coupling between the elements, which then results in a pronounced dependence of the optical response on the gap size (Figure 2a: see both far-field extinction cross sections and near-field plots for various gap distances). Specifically, rapidly decreasing the near-field coupling between the ruler elements while increasing the gap distance (Figure 2a, near-field plots on the right panel) produces a sizable blue shift in the optical extinction (Figure 2a, left panel). The so-called antibonding mode then falls into the UV region (see the feature in calculated extinction cross-section below 300 nm in Figure

2a) and produces a near-field redistribution from the gap (Figure S3b, Supporting Information). The coupling induced by linearly polarized light along the transversal axis of the ruler is far less pronounced, and the optical response correlates very weakly with the changing gap in the ruler (Figure 2b, left panel for far-field optical extinction, right panel for near-field maps), similarly to the experimental observations (Figure 1b). Overall, from a purely optical point of view, the magnetoplasmonic ruler behaves in accordance with the results of previous theoretical and experimental studies on noble-metal-based plasmon rulers.[1−12]

To quantify the performance of a plasmon ruler in reliably measuring nanogaps, we introduce a figure-of-merit (FOM), defined as the ratio between sensitivity and the width of the resonance peak, a concept that is widely used to evaluate the performance of nanoplasmonic (bio)sensors by directly correlating the biodetection sensitivity and the resolution.[34] We take two previously reported plasmon rulers as examples, the dimer nanoantenna[11] and the particle-on-the-film,[2] to extract the FOM from the reported spectroscopic data. To make the comparison straightforward, we track the measured distance for these examples in the 30−10 nm gap regime. From the data presented in Ryan et al.,[2] we find that a distance change of 10 nm between an Au nanoparticle and an Au thin film induces a 30 nm shift in the plasmon ruler peak with the full-width-half-maximum (fwhm) of 95 nm, resulting in a FOM of 0.316. Again changing the gap by 10 nm, the dimer resonance shifts by 26 nm with the corresponding shift in the fwhm from 76 to 85 nm, yielding a FOM of 0.325.[11] In addition, we fabricate Au dimer nanorulers with 150 nm nanodisks and separations of 20, 30, and 40 nm by HCL. In these rulers, we find FOMs of 0.39 and 0.31 going from 20 to 30 nm and 30 to 40 nm gaps, respectively, which is perfectly in line with extracted FOMs of previously reported ruler systems (see above). Further, it is instrumental to probe the FOM of the plasmon ruler based on the phase rather than amplitude of the plasmon modes, as the phase-based FOM is generally expected to display higher values in plasmonic sensing.[35] By modeling the phase as the first-order derivative of the amplitude of the measured optical extinction (see Figure S4, Supporting Information), we find phase-based FOM of 0.62 and 0.37 going from 20 to 30 nm and 30 to 40 nm gaps, respectively. The former is indeed slightly higher than amplitude-based FOM of the ruler.

As the next step, we demonstrate the superior operation of the magnetoplasmonic ruler, which proves to be almost 2 orders of magnitude better in terms of the FOM than the plasmonic rulers. We probe the magnetoplasmonic ruler using longitudinal MOKE (L-MOKE) spectroscopy.[25] Figure 3 shows the schematics of the measurement geometries used for this purpose. For each of the polarization states (p and s; Figure 3a,b and c,d, respectively) in L-MOKE, there are two available orientations of the electric field of light and the externally applied magnetic field with respect to the ruler axes. We denote these p-long, p-short, s-long, and s-short, depending on the orientation of the electric field of light with respect to the ruler, or dimer, axis (long or short). Specifically, for p-polarized light, the electric field and the magnetic field are parallel (Figure 3 a,b); whereas for s-polarized light, they are orthogonal to each other (Figure 3c,d). For p-polarized light, when the ruler is illuminated at 25° from the plane of incidence of the light (the plane marked in orange in all panels of Figure 3), the $\vec{E}_{inc}$ has two components $\vec{E}_x$ (along the ruler's
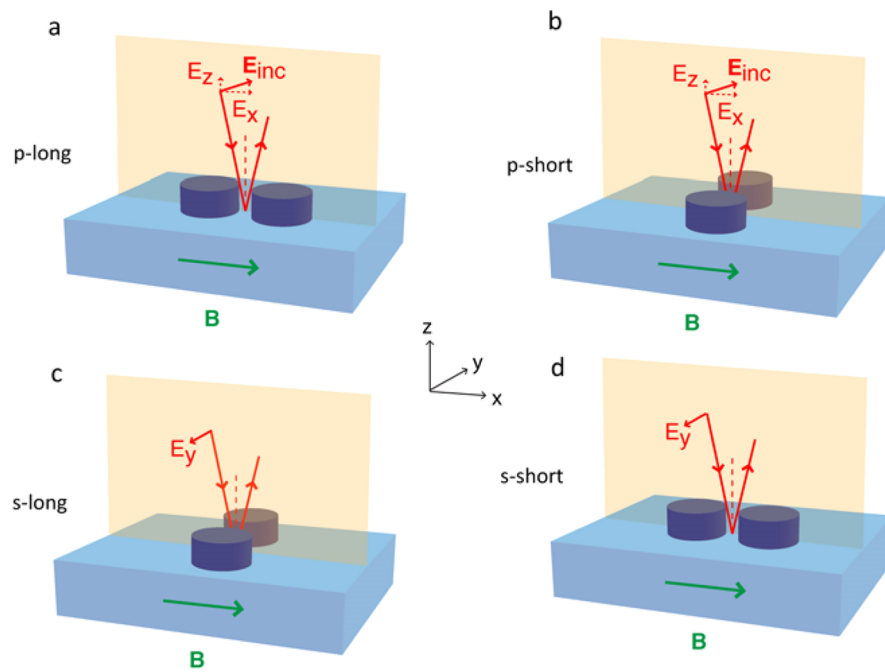
Figure 3. Schematics of the L-MOKE measurements for *p* polarization (a and b) with the electric field along the long (a) and short (b) ruler axes and *s* polarization (c and d) with electric field along the long (c) and short (d) ruler axes. The magnetic field is always along the *x* axis.
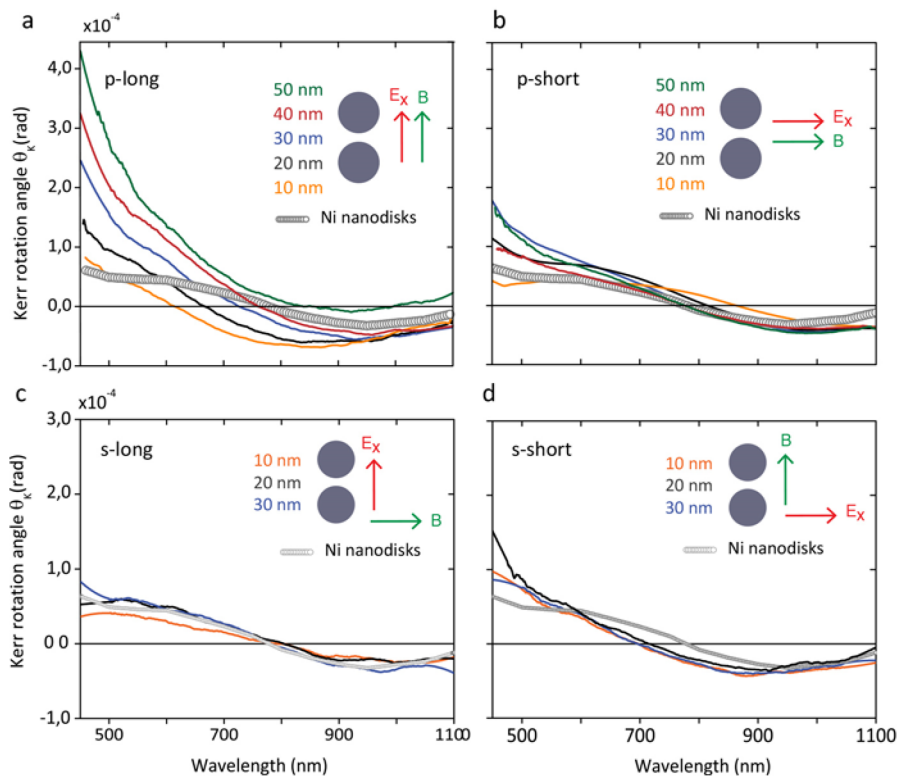
Figure 4. Spectral Kerr polarization rotation in Ni rulers with various nanogaps, along with Ni nanodisks antennas for the L-MOKE configurations described in Figure 3.

longitudinal axis) and $\vec{E}_z$. The latter, though applied to optically nonresonant mode, can efficiently couple to the magnetic field via the magneto-optical (MO) activity and induce a resonant MO dipole along the *y* direction. For *s*-polarized light, only one component of the electric field $\vec{E}_y$ is available (Figures 3c,d); this couples to the off-resonant MO dipole induced along *z*, not related to the ruler gap.[21]

The Kerr polarization rotation produced by Ni magneto-plasmonic rulers is summarized in Figure 4. Here, the differences due to the nanogap size become very pronounced, especially with *p*-polarized light (Figures 4 a, b). It can easily be seen how the Kerr rotation spectra blue shift when the nanogap is progressively reduced from 50 to 10 nm, when both magnetic field and $\vec{E}_x$ are parallel to the longitudinal ruler axis (Figure 4a,
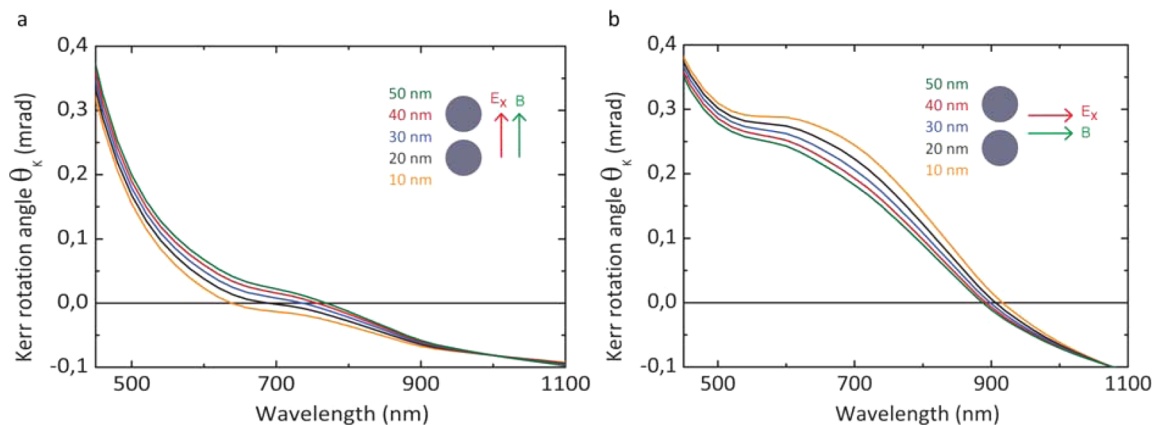
Figure 5. Calculated spectral Kerr polarization rotation in Ni rulers with 10, 20, 30, 40, and 50 nm gaps for L-MOKE in p-polarization case: *p*-long (a) and *p*-short (b) configurations.

p-long). In the *p*-short configuration (where both magnetic field and $\vec{E}_x$ are along the tangential ruler axis), a slight red shift occurs as the nanoscale distance in the ruler decreases. Similar shifts of the Kerr rotation spectra are detected with Co magnetoplasmonic rulers (Figure S6 in Supporting Information). In stark contrast with the *p* configurations, the magnetoplasmonic ruler essentially does not show any sensitivity to the nanogap size with the *s*-polarized illumination, as the Kerr polarization rotation spectra become hardly distinguishable for the various nanogap sizes (Figures 4c,d). Interestingly, from the plasmonic perspective, the light polarized along the ruler's longitudinal mode should, in principle, deliver the highest sensitivity to the nanogap size (Figure 4c, *s*-long). However, it is clear that, magnetoplasmonically, the mutual orientation of the electric field of the light and the magnetization has much greater significance. Note that in all panels of Figure 4, we also plot the Kerr polarization rotation spectra for a simple nanodisk array (dotted data) in order to give a side-to-side comparison. In this way, an immediate visual sense of how much the ruler response is altered compared to a nanodisk antenna for each gap size can be obtained. As an addition, in Figure 7S (Supporting Information), we demonstrate that the magnetoplasmonic ruler delivers excellent accuracy in nanogap resolution for 10−30 nm regime over the entire visible spectral range, as evidenced by the error bars that result from the calculated standard deviation of multiple spectral scans. This kind of statistical analysis models realistic solution-based plasmon ruler systems and provides a reliable test of the robustness of the nanogap probing with the MOKE. Note that the standard deviation, defining the performance of the ruler when taking the mean Kerr rotation per measured distance, is essential in the definition of the FOM for the magnetoplasmonic ruler, as discussed below.

To elucidate the electromagnetic details of the magnetoplasmonic ruler operation, we perform analytical calculations of the MOKE response (Figure 5). To explore the underlying physics, we generalize the model developed by De Sousa et al. for interacting magnetoplasmonic dimers.[26] For *p*-polarized light, we here have all three plasmonic resonances contributing to the longitudinal magneto-optical Kerr effect of the rulers, whereas De Sousa et al. dealt with the special case where the driving field is always perpendicular to the dimer longitudinal axis, resulting in only one active plasmon resonance. In the model, we consider an isolated dimer ruler embedded in a homogeneous dielectric medium with $n = 1$, with the ruler built

of two identical Ni oblate ellipsoids[28] (see Supporting Information for details). Once we obtain the polarizability for the single oblate nanoparticle and are able to describe each disk as a point dipole, the interaction between the two dipoles in the ruler is mediated by the Green tensor, G, which is given in its dimensionless form by[28]

$$\frac{e^{ikR}}{kR}\left[\frac{(kR)^2 + i(kR) - 1}{(kR)^2}\tilde{I} + \frac{-(kR)^2 - i(kR) + 3}{(kR)^2}\frac{R \otimes R}{R^2}\right] \tag{1}$$

where R is the vector connecting the two nanodisk centers and k is the wavevector of the incoming light. Each dipole feels the incident driving field plus the field generated by the other dipole, so that the system of equations to be solved is

$$\mathbf{p}_1 = \tilde{\alpha}_1[\mathbf{E}_0 + \tilde{G}\mathbf{p}_2] \tag{2}$$

$$\mathbf{p}_2 = \tilde{\alpha}_2[\mathbf{E}_0 + \tilde{G}\mathbf{p}_1] \tag{3}$$

Here, $\mathbf{p}_1 = \mathbf{p}_2$ and $\tilde{\alpha}_1 = \tilde{\alpha}_2$, so the equation to be solved reduces to

$$\mathbf{p} = \tilde{\alpha}[\mathbf{E}_0 + \tilde{G}\mathbf{p}] = \frac{\tilde{\alpha}}{\tilde{I} - \tilde{\alpha}\tilde{G}}\mathbf{E}_0 = \tilde{\alpha}_G\mathbf{E}_0 \tag{4}$$

The matrix $\tilde{\alpha}_G$ contains off-diagonal elements, which describe the magneto-optical activity of a single ruler. If we assume that the light propagates along the *z* axis and the $\mathbf{E}_0$ oscillates along the *x* axis (longitudinal ruler axis for the *p*-long and *s*-short configurations in Figure 3), we obtain the ruler polarizability $\tilde{\alpha}_G$ as

$$\begin{bmatrix} \alpha_{\parallel} & 0 & 0 \\ 0 & \alpha\uparrow & \alpha_{S.O.}\alpha_{\parallel}\alpha\uparrow \\ 0 & \alpha_{S.O.}\alpha_{\parallel}\alpha\uparrow & \alpha\uparrow \end{bmatrix} \tag{5}$$

where $\alpha_{\parallel}$ is the polarizability when $\mathbf{E}_0$ is parallel to the longitudinal ruler axis, and $\alpha\uparrow$ the polarizability when $\mathbf{E}_0$ is perpendicular to it; α_{SO} is a proportionality constant accounting for the bulk magneto-optical properties of Ni.[29] Earlier, for the *p*-long configuration (see Figure 3a), we saw that the optical extinction $Ext \sim \text{Im}(\alpha_{\parallel})$ red shifts as the ruler gap narrows (Figure 2a, left panel). On the other hand, the magneto-optical
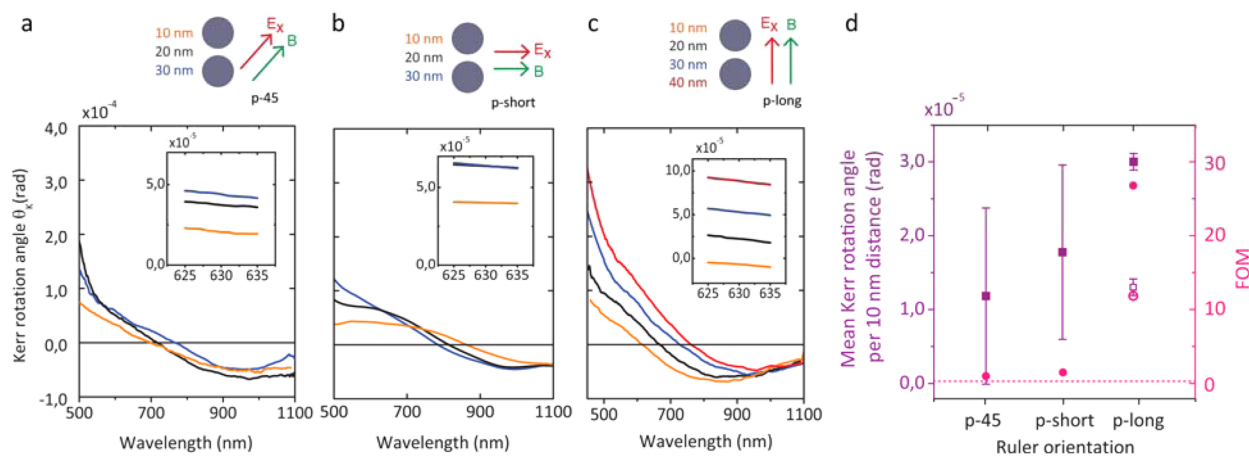
Figure 6. Evolution of the "perfect ruler" and its figure-of-merit. Kerr polarization rotation angle from magnetoplasmonic rulers, with electric and magnetic fields oriented at 45° (p-45) (a), along the tangential ruler axis (p-short) (b), and along the longitudinal ruler axis (p-long) (c). Insets (a−c): corresponding zoomed views into the 625−635 nm spectral region. (d) Mean Kerr rotation per 10 nm for the three configurations (p-45, p-short, and p-long) (left axis) and the corresponding FOMs (right axis). Solid symbols −10−30 nm nanogaps regime, open symbols −10−40 nm nanogaps regime. Dotted line: FOM of the plasmon rulers, estimated from refs 7 and 10.

Kerr rotation angle is proportional to the transverse polarizability[19]

$$\theta_{\mathrm{K}} \sim Re\left[\frac{p_y}{p_x}\right] \sim Re\left[\frac{\alpha_{\mathrm{SO}}\alpha_{\parallel}\alpha_{\uparrow}}{\alpha_{\parallel}}\right] = Re[\alpha_{\mathrm{SO}}\alpha_{\uparrow}] \tag{6}$$

and we observe a blue shift of the magnetoplasmonic features upon decreasing the gap size (Figure 4a and 5a). In the p-short configuration (Figure 4b), we do not observe higher variation of the magneto-optical response with the gap size. Comparing the experimental Kerr rotation with the analytical model overall gives a good agreement also in the p-short configuration (compare Figure 4b and 5b), though the variation is not linear over large portions of the spectra, making it harder to use this configuration as a ruler for nanodistance measurements.

We now turn to highlighting the *active operation mode* that is an intrinsic feature of the magnetoplasmonic ruler. Figure 6 follows the sequence of spatial orientations of the ruler with respect to the applied magnetic field. From all the spectroscopic MOKE data, we select the spectral region of 625−635 nm since it contains the most common laser lines in single-wavelength MOKE experiments (see the insets in Figure 6a−c). We see that the rulers at intermediate angles (45° in the p-45 case in Figure 6a and 90° in the p-short case in Figure 6b), though capable of resolving the nanogap excellently in some spectral regions, fail to do so reliably in the selected most affordable spectral range (see the insets of Figures 6a, b). The most stable configuration of the ruler—that is, p-long (Figure 6c), which it would potentially adopt in solution by aligning its easy magnetization axis (the longitudinal axis of the ruler) for magnetic fields above magnetic saturation—shows a remarkable resolution of the nanogaps up to 40 nm (see the inset of Figure 6c). This is summarized in Figure 6d (left axis), where all three orientations of the ruler are compared against the mean Kerr rotation per 10 nm distance in the nanogap. Both higher absolute rotations per distance and the smallest error in mean rotation variation in 10−40 nm nanogap regime are achieved here with the p-long configured ruler. The latter essentially makes this magnetoplasmonic system a "perfect ruler" in the conventional sense, that is, a ruler designed to measure both small and large distances with exactly the same

precision (see the nearly equidistant Kerr rotation features on the inset of Figure 6c). This becomes clearly visible when we spectrally map the sensitivity of the Kerr polarization rotation angle ($\Delta\Theta_{\mathrm{K}}$) to the distance change of 10 nm (Figure S8 in the Supporting Information), which is practically flat in the 628−633 nm wavelength range. In order to gauge the performance of the regular plasmon and magnetoplasmonic rulers, we define a dimensionless FOM for magnetoplasmonics as the mean change in Kerr polarization rotation angle $\Delta\Theta_{\mathrm{K}}$ induced by a distance change of 10 nm, divided by the standard deviation (SD) of $\Delta\Theta_{\mathrm{K}}$, taken as a measurement precision or the resolution in the MOKE experiment (similar to the fwhm of the plasmon peak, but conceptually different from the signal-to-noise ratio)

$$\mathrm{FOM} = \frac{\langle\Delta\Theta_{\mathrm{K}}\rangle}{\mathrm{SD}(\Delta\Theta_{\mathrm{K}})} \tag{7}$$

Tracking the FOM values for all ruler orientations conservatively in the 10−30 nm nanogap regime (pink data points and the right axis of Figure 6d) and comparing these to the highest of previously estimated FOMs for the regular plasmon rulers (∼0.62, marked with a dotted line in Figure 6d), we see that not only do the FOMs of magnetoplasmonic rulers in basically any orientation exceed those of the regular plasmon rulers (the p-45 orientation gives an FOM of 1.0 and a p-short of 1.5) but that, with both electric field and magnetization aligned along the longitudinal axis of the magnetoplasmonic ruler—that is, the p-long orientation—the FOM in measuring nanoscopic distances in 10−30 regime reaches 26.7, which exceeds the performance of regular plasmon rulers by roughly 2 orders of magnitude (Figure 6d, right axis). Extending it to 10−40 regime (as in Figure 6c), we earn FOM of 12 (open symbols in Figure 6d). As we continue to add larger distances, naturally, the sensitivity of the ruler drops, alongside with increasing standard deviation in Kerr polarization rotation measurements due to nanofabrication particularities of the nanodimers with such large nanogaps by HCL (see Supporting Information), where the lateral separation of individual rulers essentially becomes smaller than the nanogap. Still, even in 10−50 nm regime the FOM of magnetoplasmonic ruler reaches 5,

an order of magnitude exceeding the regular plasmon rulers FOM.

Apart from the potential intrinsic ability to realign itself during the measurements (for example, in a liquid environment) to adopt the best possible signal resolution and FOM, a situation where the application of the magnetic field at saturation does not readily reorient the ruler can be envisaged. For example, this could be realized in strongly viscous environments or when the ruler is bound to a certain molecular structure. In this case, increasing the magnetic field and simultaneously probing the ruler's spectral polarization rotation response would track the spatial reorientation of the ruler in real time, which would eventually reach its fully aligned configuration. In this scenario, several physical parameters of the embedding medium could be probed, apart from the nanogap reading. These might include the characterization of its viscosity and the various tensile stresses a biochemical system might experience, possibly also providing hints on the dynamic evolution of the structure and the composition. The possibility for the encapsulation of Ni with Au prompts us to envision the scenario of the practical use of the active magnetoplasmonic ruler, where a thin Au layer is created at the surface of metal ferromagnetic nanoparticles, similarly to already widely employed core−shell gold−ferromagnetic oxide theranostic agents. Another Ni biofunctionalization protocol suggesting polyhistidine peptides as purifying agents[30] may also be foreseen. In the envisaged use of magnetoplasmonic rulers in solution, both nanoparticles in the ruler would acquire a magnetic moment with the application of the external magnetic field and would experience attractive forces due to the magnetic dipolar interaction, subjecting the (bio)matter in the ruler gap to mechanical stress by actuation. The attractive force will also be strongest (from pN up to nN) when the ruler reaches the "perfect" orientation. By proper magnetoplasmonic ruler design, magnetic field-induced orientation and mechanical actuation would be used simultaneously to implement a conceptual device for the nanocharacterization of the elastoplastic properties of soft matter. This would allow probing of multidimensional length variations in molecular systems with subnanometer precision under the application of precisely controlled external stimuli. In practice, the field control of the force exerted by the nanoparticles in the ruler can be readily achieved by using systems with magnetic moment proportional to magnetic field. This could be realized in various ways, for example, by using nanostructures made of a Py (permalloy)/Cu/Co trilayer. By tuning the Cu spacer thickness, the Py and Co nanodisks could be antiferromagnetically exchange-coupled in each element of the ruler at zero field, giving a net zero magnetic moment.[31,32] This means that the material inside the ruler gap would experience no mechanical stress. As the external magnetic field is ramped up, the two magnetic submoments in each element of the ruler would being to rotate in opposite direction, such that the angle between them progressively changes from 180° to 0°, leading to a total magnetic moment proportional to the applied field, and precisely controlled by it. Such magnetic moment induction then translates to mechanical stress in the ruler gap, which is in turn precisely controlled by the external magnetic stimuli. Another alternative is use simple Py nanodisk elements that can be individually designed to form a so-called magnetic vortex state. In this case too, in the absence of an externally applied magnetic field, the magnetic moment of each nanodisk is negligibly small, and it is only when the field is applied that a magnetic moment proportional to magnetic field is induced by the distortion of the vortex configuration.[33] This second approach implies the use of much simpler ruler structures; however, the moment induced in the nanodisk units is much smaller (in the linear regime, i.e. where $\mu \propto H$) than that achievable through multilayered ruler elements. In principle, this difference can be turned into an advantage, as it implies that a spectrum of opportunities exists from which to devise a nanoscale elastoplastic molecular characterization tool, designed by selecting the proper ruler structure and depending on the required force range. Importantly, neither design affects the core magnetoplasmonic ruler principle of nanoscale distance measurement, discussed above.

In general, it appears that the potential extension of the active magnetoplasmonic ruler concept to colloidal nanoparticles in a biological environment is within the practical reach. Besides the scenarios we described above, the assembly of nanoparticles in solution can now be guided by light with precisely controlled separations.[36] Further, a very recent study on magnetic hydrogel for clinic applications demonstrates how colloidal magnetic nanoparticles, suspended in a hydrogel, are controllably organized in chains with alternating magnetic field.[37] With the already mentioned number of studies on the biocompatibility of magnetic nanoparticles, and the availability of various core−shell geometries, accommodating the ferromagnetic functionalities also with the possibility of direct biofunctionalization of the ferromagnetic metallic nanostructures, we overall expect the magnetoplasmonic rulers to meet similar challenges as their plasmonic counterparts. That is, the exact positioning/delivery and optical signal read-out, often obstructed by the strong absorption in biological media, would be the issues to address for both types of rulers. However, magnetoplasmonic rulers deliver the clear advantage of the active operation, outlined above, which can also be employed to solve the mentioned challenges, for example, with precision delivery.

In summary, we have developed a new type of a magnetic field-activated plasmon ruler that reports nanogap distances via Kerr polarization rotation. The features of this system include its robustness in nanogap measurements over a broad spectral range, the capacity to report both small and larger nanoscale distances with about 2 orders of magnitude better FOM than regular plasmon rulers, and its intrinsic ability to adopt the spatial orientation best suited for the nanogap measurements, something we call signal amplification by spatial orientation. All these features are realized in a highly parallel fashion; that is, all magnetoplasmonic rulers of the measured ensemble would necessarily adopt a nominally identical orientation. This allows us to envision such rulers being employed not only for highly sensitive determination of nanoscale distances but also as versatile nanotools for characterizing soft matter by dynamically tracking the elastic and other physical properties of various biological and chemical media.

■ ASSOCIATED CONTENT

Ⓢ Supporting Information

Rulers nanofabrication, optical extinction and modeling extinction cross-sections of the rulers, extinction spectra, schematic charge distribution of the hybridized plasmon modes of the dimer ruler and calculated optical extinction cross sections spectra for the rulers, optical and MOKE simulations, near-field plots of longitudinal bonding and antibonding modes, plasmon Au dimer nanorulers, exper-

imental optical extinction spectra and simulated respective phases, the simulated phases of longitudinal resonances in Au rulers, Kerr rotation Θ_K spectra of Co rulers, normalized Kerr rotation, spectrally resolved sensitivity of the ruler, and hysteresis loops of Ni nanodimer rulers. The Supporting Information is available free of charge on the ACS Publications website at DOI: 10.1021/acs.nanolett.5b00372.

■ AUTHOR INFORMATION

Corresponding Authors
*E-mail: irina.zubritskaya@chalmers.se.
*E-mail: n.maccaferri@nanogune.eu.
*E-mail: alexd@chalmers.se. Phone: +46-31-7725177.

Author Contributions
I.Z., K.L., and A.D. devised the concept. I.Z. performed all nanofabrication and optical, MOKE experimental measurements. R.D. performed AGM measurements. N.M. and P.V. performed numerical simulations and analytical calculations. I.Z., N.M., P.V., and A.D. wrote the manuscript. All authors contributed to the discussions.

Notes
The authors declare no competing financial interest.

■ REFERENCES

(1) Sönnichsen, C.; Reinhard, B. M.; Liphardt, J.; Alivisatos, A. P. *Nat. Biotechnol.* **2005**, *23*, 741−745.
(2) Hill, R. T.; Mock, J. J.; Hucknall, A.; Wolter, S. D.; Jokerst, N. M.; Smith, D. R.; Chilkoti, A. *ACS Nano* **2012**, *6*, 9237−9246.
(3) Prashant, K. J.; Huang, W.; A. El-Sayed, M. *Nano Lett.* **2007**, *7*, 2080−2088.
(4) Na Liu, L.; Hentschel, M.; Weiss, T.; Alivasatos, A. P.; Giessen, H. *Science* **2011**, *332*, 1407−1410.
(5) Rechberger, W.; Hohenau, A.; Leitner, A.; Krenn, J. R.; Lamprecht, B.; Aussenegg, F. R. *Opt. Commun.* **2003**, *220*, 137−141.
(6) Norlander, P.; Oubre, C.; Prodan, E.; Li, K.; Stockman, M. I. *Nano Lett.* **2004**, *4*, 899−903.
(7) Wang, J.; Boriskina, S. V.; Wang, H.; Reinhard, B. M. *ACS Nano* **2011**, *5*, 6619−6628.
(8) Yang, L.; Wang, H.; Yan, B.; Reinhard, B. M. *J. Phys. Chem. C* **2010**, *114*, 4901−4908.
(9) Anker, J. N.; Hall, W. P.; Lyandres, O.; Shah, N. C.; Zhao, J.; Van Duyne, R. P. *Nat. Mater.* **2008**, *7*, 442−452.
(10) Sheikholeslami, S.; Jun, Y.-W.; Jain, P. K.; Alivisatos, A. P. *Nano Lett.* **2010**, *10*, 2655−2660.
(11) Acimovic, S. S.; Kreuzer, M. P.; González, M. U.; Quidant, R. *ACS Nano* **2009**, *3*, 1231−1237.
(12) Gunnarsson, L.; Rindzevicius, T.; Prikulis, J.; Kasemo, B.; Käll, M.; Zou, S.; Schatz, G. C. *J. Phys. Chem. B* **2005**, *109*, 1079−1087.

(13) Kuzyk, A.; Schreiber, R.; Zhang, H.; Govorov, A. O.; Liedl, T.; Na Liu, L. *Nat. Mater.* **2014**, *13*, 862−866.
(14) Bardhan, R.; Lal, S.; Joshi, A.; Halas, N. J. *Acc. Chem. Res.* **2011**, *44*, 936−946.
(15) Tajon, C. A.; Seo, D.; Asmussen, J.; Shah, N.; Jun, Y.-W.; Craik, C. S. *ACS Nano* **2014**, *8*, 9199−9208.
(16) Chen, J.; Albella, P.; Pirzadeh, Z.; Alonso-González, P.; Huth, F.; Bonetti, S.; Bonanni, V.; Åkerman, J.; Nogúes, J.; Vavassori, P.; Dmitriev, A.; Aizpurua, J.; Hillenbrand, R. *Small* **2011**, *7*, 2341−2347.
(17) Zvezdin, A. K.; Kotov, V. A. *Modern Magnetooptics and Magnetooptical Materials*; Taylor & Francis: New York, 1997.
(18) Bonanni, V.; Bonetti, S.; Pakizeh, T.; Pirzadeh, Z.; Chen, J.; Nogúes, J.; Vavassori, P.; Hillenbrand, R.; Åkerman, J.; Dmitriev, A. *Nano Lett.* **2011**, *11*, 5333−5338.
(19) Maccaferri, N.; Berger, A.; Bonetti, S.; Bonanni, V.; Kataja, M.; Hang Qin, Q.; van Dijken, S.; Pirzadeh, Z.; Dmitriev, A.; Nogúes, J.; Åkerman, J.; Vavassori, P. *Phys. Rev. Lett.* **2013**, *111*, 167401.
(20) Papaioannou, E. T.; Kapaklis, V.; Patoka, P.; Giersig, M.; Fumagalli, P.; Garcia-Martin, A.; Ferreiro-Vila, E.; Ctistis, G. *Phys. Rev. B* **2010**, *81*, 054424.
(21) Lodewijks, K.; Maccaferri, N.; Pakizeh, T.; Dumas, R.; Zubritskaya, I.; Åkerman, J.; Vavassori, P.; Dmitriev, A. *Nano Lett.* **2014**, *14*, 7207−7214.
(22) Ctistis, G.; Papaioannou, E.; Patoka, P.; Gutek, J.; Fumagalli, P.; Giersig, M. *Nano Lett.* **2009**, *9*, 1−6.
(23) González-Díaz, J. B.; Sepúlveda, B.; García-Martín, A.; Armelles, G. *Appl. Phys. Lett.* **2010**, *97*, 043114.
(24) Fredriksson, H.; Alaverdyan, Y.; Dmitriev, A.; Langhammer, C.; Sutherland, D. S.; Zäch, M.; Kasemo, B. *Adv. Mater.* **2007**, *19*, 4297−4302.
(25) Vavassori, P. *Appl. Phys. Lett.* **2000**, *77*, 1605−1607.
(26) de Sousa, N.; Froufe-Pérez, L. S.; Armelles, G.; Cebollada, A.; González, M. U.; García, F.; Meneses-Rodríguez, D.; García-Martín, A. *Phys. Rev. B* **2014**, *B 89*, 205419.
(27) Maccaferri, N.; González-Díaz, J. B.; Bonetti, S.; Berger, A.; Kataja, M.; Sebastiaan van, Dijken; Nogúes, J.; Bonanni, V.; Pirzadeh, Z.; Dmitriev, A.; Åkerman, J.; Vavassori, P. *Opt. Express* **2013**, *21*, 9875−9889.
(28) Depasse, F.; Vigoureux, J. M. *J. Phys. D: Appl. Phys.* **1994**, *27*, 914−919.
(29) Maccaferri, N.; Kataja, M.; Bonanni, V.; Bonetti, S.; Pirzadeh, Z.; Dmitriev, A.; Sebastiaan van, Dijken; Åkerman, J.; Vavassori, P. *Physica Status Solidi A* **2014**, *211*, 1067−1075.
(30) Hochuli, E.; Bannwarth, W.; Döbeli, H.; Gentz, R.; Stüber, D. *Nat. Biotechnol.* **1988**, *11*, 1321−1325.
(31) Vavassori, P.; Bonanni, V.; Busato, A.; Bisero, D.; Gubbiotti, G.; Adeyeye, A. O.; Goolaup, S.; Singh, N.; Spezzani, C.; Sacch, M. *J. Phys. D: Appl. Phys.* **2008**, *41*, 134014.
(32) Bonanni, V.; Bisero, D.; Vavassori, P.; Gubbiotti, G.; Madami, M.; Adeyeye, A. O. *J. Magn. Magn. Mater.* **2009**, *321*, 3038−3041.
(33) Grimsditch, M.; Vavassori, P.; Novosad, V.; Metlushko, V.; Shima, H.; Otani, Y.; Fukamichi, K. *Phys. Rev. B* **2002**, *65*, 172419.
(34) Nanoplasmonic Sensors. *Integrated Analytical Systems*; Dmitriev, A. Ed.; Springer: New York, 2012.
(35) Lodewijks, K.; Van Roy, W.; Borghs, G.; Lagae, L.; Van Dorpe, P. *Nano Lett.* **2012**, *14*, 1655−9.
(36) Herrmann, L. O.; Valev, V. K.; Tserkezis, C.; Barnard, J. S.; Kasera, S.; Scherman, O. A.; Aizpurua, J.; Baumberg, J. J. *Nat. Commun.* **2014**, *5*, 4568.
(37) Hu, K.; Sun, J.; Guo, Z.; Wang, P.; Chen, Q.; Ma, M.; Gu, N. *Adv. Mater.* **2015**, *27*, 2507−14.